LETTER

https://doi.org/10.1038/s41586-019-1117-3

Neurocranial development of the coelacanth and the evolution of the sarcopterygian head

Hugo Dutel[1,2]*, Manon Galland[3], Paul Tafforeau[4], John A. Long[5], Michael J. Fagan[1], Philippe Janvier[6], Anthony Herrel[7], Mathieu D. Santin[8], Gaël Clément[6] & Marc Herbin[7]

The neurocranium of sarcopterygian fishes was originally divided into an anterior (ethmosphenoid) and posterior (otoccipital) portion by an intracranial joint, and underwent major changes in its overall geometry before fusing into a single unit in lungfishes and early tetrapods[1]. Although the pattern of these changes is well-documented, the developmental mechanisms that underpin variation in the form of the neurocranium and its associated soft tissues during the evolution of sarcopterygian fishes remain poorly understood. The coelacanth *Latimeria* is the only known living vertebrate that retains an intracranial joint[2,3]. Despite its importance for understanding neurocranial evolution, the development of the neurocranium of this ovoviviparous fish remains unknown. Here we investigate the ontogeny of the neurocranium and brain in *Latimeria chalumnae* using conventional and synchrotron X-ray micro-computed tomography as well as magnetic resonance imaging, performed on an extensive growth series for this species. We describe the neurocranium at the earliest developmental stage known for *Latimeria*, as well as the major changes that the neurocranium undergoes during ontogeny. Changes in the neurocranium are associated with an extreme reduction in the relative size of the brain along with an enlargement of the notochord. The development of the notochord appears to have a major effect on the surrounding cranial components, and might underpin the formation of the intracranial joint. Our results shed light on the interplay between the neurocranium and its adjacent soft tissues during development in *Latimeria*, and provide insights into the developmental mechanisms that are likely to have underpinned the evolution of neurocranial diversity in sarcopterygian fishes.

Although the coelacanth *Latimeria* has been studied extensively since its discovery 80 years ago[4], most aspects of its cranial development remain unknown[2]. This lack of knowledge is largely due to the scarcity of embryonic material and—until recently—the absence of efficient non-invasive methods of studying the internal anatomy of these rare specimens. Here we digitized five specimens of this ovoviviparous species that ranged from prenatal to postnatal developmental stages: a small fetus (5 cm total length), a pup with a yolk sac (hereafter referred to as P1, 30.5 cm total length), a pup whose yolk sac is resorbed (hereafter referred to as P2, 35.6 cm total length), a juvenile (42 cm total length) and an adult (132 cm total length) (Fig. 1). To the best of our knowledge, these specimens represent the most complete growth series currently available for this species.

In the fetus, the neurocranium is already divided into two portions at the level of the ventral fissure and the intracranial joint (Figs. 1, 2, Extended Data Fig. 1). The individualization of the two divisions of the neurocranium thus occurs earlier, probably during early embryonic development. The ethmosphenoid portion of the neurocranium is much narrower and slightly longer than the otoccipital portion, and lengthens during prenatal development (Figs. 2, 3, Extended Data Fig. 1). The trabeculae extend anteroventrally to the notochord, and delimit the open hypophyseal fossa. They fuse anteriorly as a narrow trabeculae communis (Fig. 2, Extended Data Figs. 1, 2). Posteriorly, the ethmosphenoid portion develops around the anterior notochordal tip in the fetus; in later stages, it lies entirely anterior to the notochord. The notochord penetrates the ethmosphenoid portion at a position posterodorsal to the trabeculae, and terminates posterior to the hypophysis, the foramina for the internal carotids, the pituitary vein and the oculomotor nerve (Fig. 2, Extended Data Figs. 1–3). At this level, the neurocranium shows a marked curvature under the cephalic flexure. This region is similar in topographic terms to the condition that is observed in other gnathostomes, in which it is interpreted as deriving from the orbital cartilage[5–7]. A shallow dorsum sellae separates the hypophyseal fossa and the large basicranial fenestra. In the otoccipital portion, the parachordal plates are widely separated and extend anteriorly as a short otic shelf. The otic region is shallow and the commissura prefacialis is open, as is the metotic fissure in the posterior wall of the otic capsule (Fig. 2, Extended Data Fig. 1).

The configuration of the neurocranium and brain observed in the fetus is, to our knowledge, unique among gnathostomes[6,7]. The endocranial cavity reaches the neurocranial floor in the ethmosphenoid portion, but continues dorsally to the notochordal canal in the otoccipital portion (Figs. 2, 3, Extended Data Figs. 1–3). The cerebellum and mesencephalon straddle the anterior and posterior divisions, and are positioned dorsally to the forebrain and the ethmosphenoid portion. The short pila antotica meets the orbital cartilage ventral to the mesencephalon, and the trochlear nerve emerges above the eyes (Fig. 2, Extended Data Fig. 1). Dorsally, the neurocranium is largely incomplete around the cerebellum and the mesencephalon, and the taenia marginalis posterior fails to reach the orbital cartilage. Later during prenatal development, the endocranium of the ethmosphenoid portion moves dorsally as a narrow internasal septum develops, such that P1 presents a tropibasic neurocranium (Fig. 3, Extended Data Figs. 2, 3). The ethmoidal region is proportionally shorter in the fetus compared to the adult, because the cavity for the rostral organ is not yet formed (Figs. 2, 3, Extended Data Fig. 1). Only from the stage represented by P1 onwards is the cavity for the rostral organ separated from the endocranial cavity, which is steeply depressed in its anterior portion (Fig. 3, Extended Data Fig. 3). The expansion of the rostral organ remodels the ethmoid region, and displaces the ethmoidal articulation from the postnasal wall (in the fetus) to the lateral side of the nasal capsules (in later stages) (Figs. 2, 3, Extended Data Fig. 1).

The reduction in the relative size of the brain (Extended Data Table 1) and changes in its shape (Fig. 3, Extended Data Figs. 3, 4) are associated with a progressive displacement towards the otoccipital portion. In the fetus (Figs. 2, 3, Extended Data Figs. 1–4), the brain spans the intracranial joint and the telencephalon reaches the nasal capsules. In P1, P2

[1]School of Engineering and Computer Science, Medical and Biological Engineering Research Group, University of Hull, Hull, UK. [2]School of Earth Sciences, University of Bristol, Bristol, UK. [3]UMR 7206 (MNHN-CNRS-Université Paris Diderot), Éco-Anthropologie et Ethnobiologie, Département Homme et Environnement, Muséum National d'Histoire Naturelle, Paris, France. [4]European Synchrotron Radiation Facility, Grenoble, France. [5]College of Science and Engineering, Flinders University, Adelaide, South Australia, Australia. [6]UMR 7207 (MNHN-CNRS-Sorbonne Université), CR2P Centre de Recherche en Paléontologie-Paris, Département Origines et Évolution, Muséum National d'Histoire Naturelle, Paris, France. [7]UMR 7179 (MNHN-CNRS) MECADEV, Département Adaptations du Vivant, Muséum National d'Histoire Naturelle, Paris, France. [8]Inserm U 1127, CNRS UMR 7225, Centre for NeuroImaging Research, ICM (Brain & Spine Institute), Sorbonne University, Paris, France. *e-mail: h.dutel@bristol.ac.uk

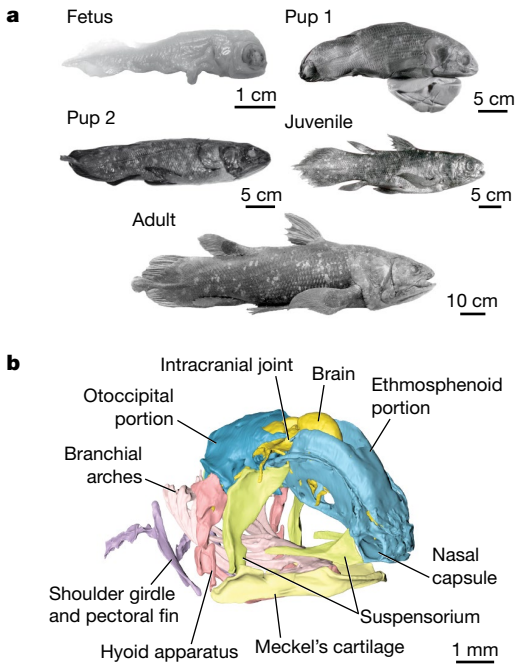

Fig. 1 | The development of the living coelacanth *L. chalumnae*. **a**, Growth series gathered for this study ($n = 5$ specimens). **b**, Overall anterolateral view of the skull of the fetus.

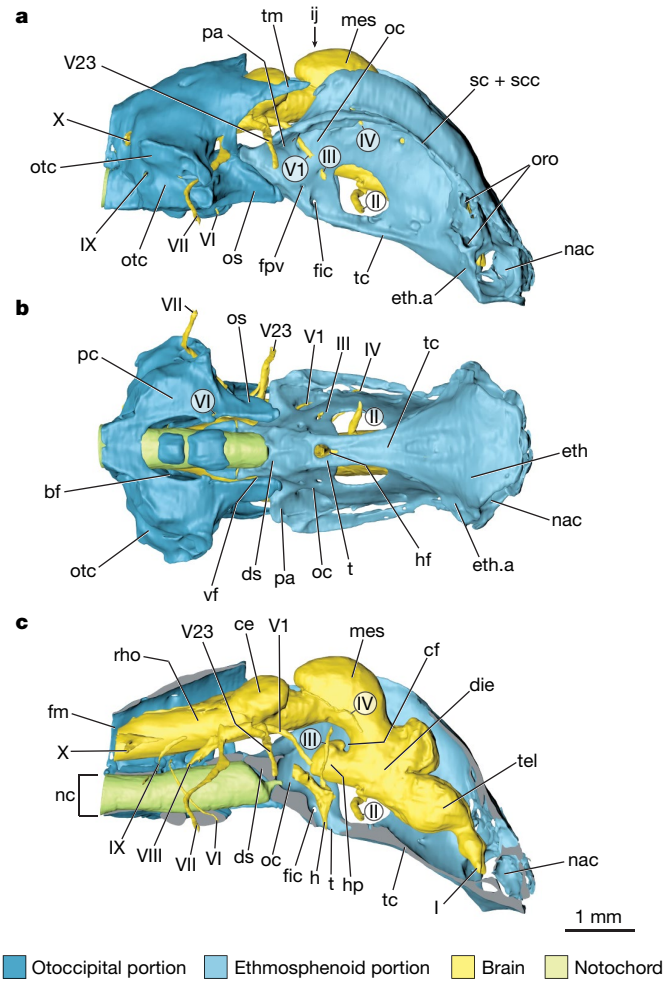

Fig. 2 | The neurocranium of *L. chalumnae* fetus. a, **b**, Neurocranium in right lateral (**a**) and ventral (**b**) views. **c**, Right lateral view of the neurocranium virtually cut open along the midsagittal plane. bf, basicranial fenestra; ce, cerebellum; cf, cephalic flexure; die, diencephalon; ds, dorsum sellae; eth, ethmoid cartilage; eth.a, ethmoidal articulation; fm, foramen magnum; fic, foramen for internal carotid artery; fpv, foramen for the pituitary vein; h, hypophysis; hf, hypophyseal fossa; hp, hypothalamus; ij, intracranial joint; mes, mesencephalon; nac, nasal capsule; nc, notochoral canal; oc, orbital cartilage; oro, opening for the rostral organ; os, otic shelf; otc, otic capsule; pa, pila antotica; pc, parachordal plate; rho, rhombencephalon; sc, supraorbital cartilage; ssc, supraorbital sensory canal; t, trabeculae; tc, trabeculae communis; tel, telencephalon; tm, taenia marginalis; vf, ventral fissure; I, olfactory nerve; II, optic nerve; III, oculomotor nerve; IV, trochlear nerve; V1, ophthalmic branch of the trigeminal nerve; V23, maxillomandibular branch of the trigeminal nerve; VI, abducens nerve; VII, facial nerve; VIII, acoustic nerve; IX, glossopharyngeal nerve (or foramen for this nerve); X, vagus nerve.

and the juvenile (Fig. 3, Extended Data Figs. 3–5), the brain represents about 11% of the endocranial volume. The telecephalon continues to span the intracranial joint but the mesencephalon is restricted to the otoccipital portion. The confinement of the brain within the otoccipital portion occurs only during postnatal development (Fig. 3, Extended Data Figs. 3, 4). In the adult (Fig. 3, Extended Data Figs. 3, 4), the entire brain is restricted to the otoccipital portion and represents 1% of the endocranial volume, as previously reported[2,3]. In the fetus, the brain is curved ventrally and the cephalic flexure is less pronounced than in other gnathostomes, as the rhombencephalon and the mesencephalon develop far-dorsal to the forebrain (Figs. 2, 3, Extended Data Figs. 1–4). This configuration is retained in P1 but not in P2, in which the brain straightens (Fig. 3, Extended Data Figs. 3, 4). In the fetus, the hypophysis and the hypothalamus are positioned vertically below the mesencephalon. They are displaced towards the telencephalon during ontogeny, as a long hypophyseal duct elongates and extends into a deep hypophyseal fossa (Fig. 3, Extended Data Figs. 3, 4). The endocranium of the fetus is proportionally broader than in other stages, and has short olfactory canals, divergent olfactory capsules and a short hypophyseal fossa (Fig. 3). These characteristics can be regarded as plesiomorphic, and are shared by stem-osteichthyans[8], early sharks and placoderms[9], and the tetrapodomorph fish *Tungsenia*[10]. From the stage represented by P1 onwards (Fig. 3), the endocranium shows the typical shape observed in sarcopterygians[9,11,12]; it has long olfactory canals, a narrow cavity located above a thin interorbital septum and a deep hypophyseal fossa that extends anteroventrally. Beyond the mismatch between the brain and the endocranium in adults, the changes in the position, relative size and shape of the brain are reflected in the endocranium throughout the ontogeny of *Latimeria*.

The size of the notochord is similar to that of the rhombencephalon in the fetus (Figs. 2, 3, Extended Data Figs. 1, 3), and is proportionally larger compared to that of other vertebrates at a similar developmental stage[6]. Only the rostral tip of the notochord is markedly reduced in size, and finishes just behind the hypophysis. Thus, the notochord probably retains its initial anterior position in the fetus. The notochordal foramen in the ethmosphenoid portion is lost in later stages as the basisphenoid ossifies; this foramen is retained in adult stem-sarcopterygians[13,14]. From the fetus to the adult, the notochord undergoes a proportionally greater degree of expansion than the brain (Fig. 3, Extended Data Fig. 3, Extended Data Table 1). Thus, the expansion of the notochord probably starts during the embryonic phase of development, and its position remains almost unchanged throughout ontogeny.

Our results illuminate the development of the neurocranial structures in *Latimeria*. The neurocranium is divided into two portions in the earliest observed stage of ontogeny, but remains topographically conservative relative to that of other gnathostomes[5–7,15]. The ethmosphenoid portion is entirely anterior to the notochord in adults, but develops partly in the prechordal domain as it includes the orbital cartilage and the rostral tip of the notochord. As such, the intracranial joint is not coincident with the limit between the mesoderm-derived and the neural-crest-derived neurocranium[15–17], but is instead posterior to it. In addition to a complete division of the neurocranium, the *Latimeria* fetus shows a unique combination of developmental characteristics. The prechordal region is proportionally much

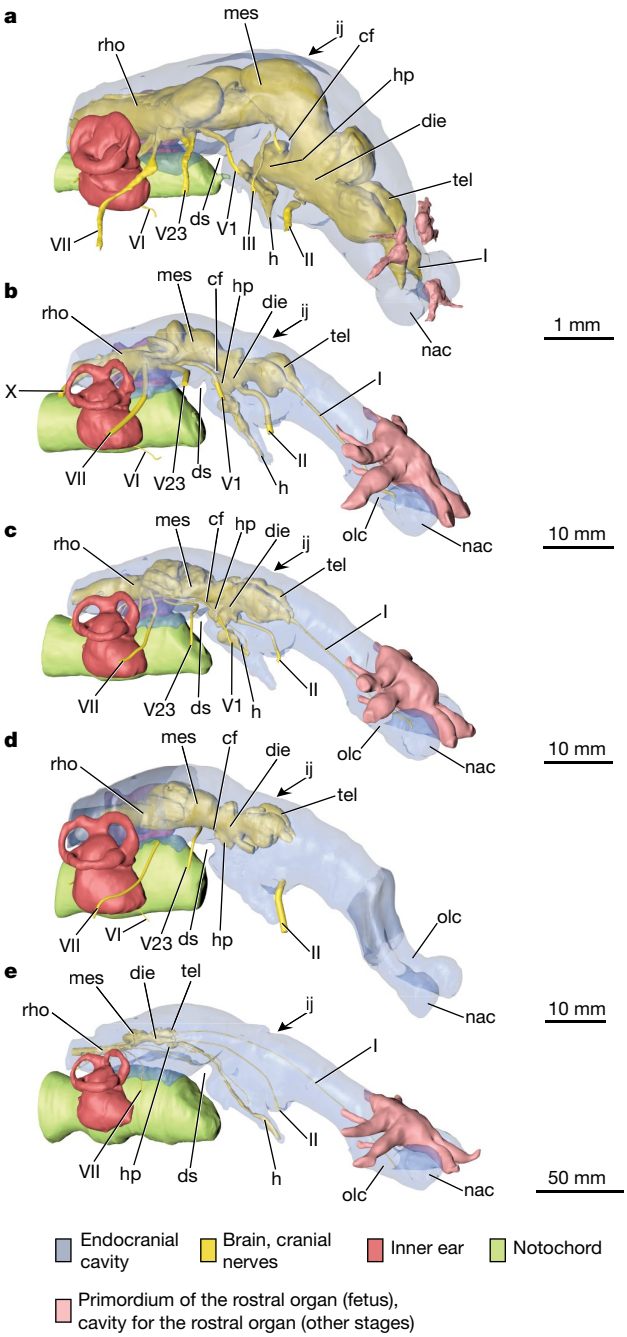

Fig. 3 | Endocranium and brain in *L. chalumnae* growth series. **a**–**d**, The fetus (**a**), P1 (**b**), P2 (**c**), juvenile (**d**) and adult (**e**) in right anterolateral view. Grey portions in the juvenile (**d**) were reconstructed based on P2 (**c**). The rostral organ was not reconstructed in **d**, because it had previously been destroyed in the dissection of the specimen (see Methods). olc, olfactory canal; other abbreviations as in Fig. 2. Sample size for each stage, $n = 1$.

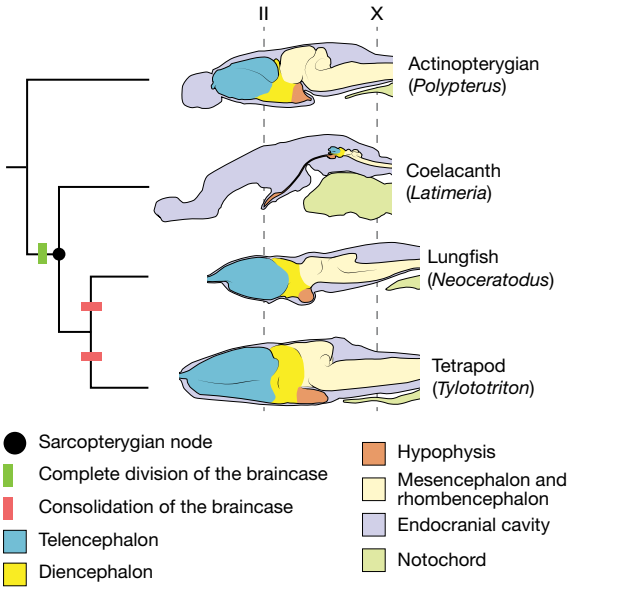

Fig. 4 | Neurocrania of selected extant osteichthyan fishes and a tetrapod. The endocrania are shown in left lateral view and aligned on the foramina for the optic (II) and vagus (X) nerves. The ancestral neurocranium of sarcopterygians is divided into two portions by the intracranial joint and the ventral fissure, and its consolidation into a single unit occurred independently in lungfishes and tetrapods. Note the position and relative size of the brain and notochord, the configuration of the brain and the orientation of the hypophysis in *Latimeria* with respect to other taxa. *Neoceratodus* is redrawn from refs [19,27]. Juvenile *Polypterus* and *Tylototriton* are drawn from acquisitions of propagation phase-contrast X-ray synchrotron micro-tomography (PPC-SRμCT), and the adult *Latimeria* is drawn based on Extended Data Fig. 3.

narrower than in embryos of lungfishes[6,18], *Polypterus*, *Amia* and amphibians[6,7], in which the trabeculae are widely separated and in line with the parachordal plates. In these taxa, the brain straightens as it folds extensively during early ontogeny, allowing its encapsulation within the neurocranium[19]. The configuration of the brain in the *Latimeria* fetus derives from this general pattern and—together with the deep dorsum sellae[20]—probably results from the enlargement of the notochord. The development of the latter is markedly altered in *Latimeria* compared to other living vertebrates (Fig. 4), in which the notochord always reduces and retracts from the hypophyseal region relatively early in development[6,7,21].

The development of the notochord observed in *Latimeria* appears to affect the adjacent tissues, and might underpin the complete division of the neurocranium. By remaining in an anterior position and expanding in early ontogeny, the notochord probably broadly separates the parachordal plates, and anteriorly restricts the narrow trabecular plate and the orbital cartilage. Consequently, the fusion of these cartilages with the parachordal plates might be hindered, which would result in the formation of a ventral fissure. As the notochord expands, the hindbrain and midbrain are displaced to a position dorsal to the ethmosphenoid portion; their volume probably affects the patterning of the adjacent neurocranial roof. We therefore suggest that the intracranial joint probably results from the configuration of the brain as imposed by the notochord. Accordingly, the complete division of the braincase is always associated with a very large notochord in contact with the dorsum sellae, a deep hypophyseal fossa and a relatively narrow hypophyseal region of the braincase with respect to the otoccipital division[1,9,22]. The modulation of the growth trajectories of the brain and notochord might also allow the persistence of a ventral fissure when the intracranial joint is consolidated, as in *Youngolepis*[23].

A discrepancy between the brain and the endocranial cavity exists in various fishes[24,25], but the magnitude of the mismatch observed in adult *Latimeria* is—to our knowledge—unequalled among living vertebrates. In living gnathostomes, the forebrain lengthens anterior to the eyes above the trabecular plate, as the hypophysis expends posteriorly[26] (Fig. 4). This early developmental pattern appears to be shared by *Latimeria*, given the position of the forebrain in the fetus and its proportions in adults (Figs. 2, 3, Extended Data Figs. 3, 4). However, the notochord later fills up the space behind the hypophyseal fossa that, in other gnathostomes, is mostly occupied by the brain (Fig. 4). The marked expansion of the notochord thus probably causes a major spatial packing constraint on the brain, and anteriorly restricts the growth of the hypophyseal and orbital regions, which might drive the allometric growth and elongation of the brain. The similarities between

the endocranium of *Latimeria* pups and those of stem-sarcopterygians[9,12–14] suggest that this developmental pattern is ancestral to the group, whereas brain shape appears to match that of the endocranium in fossil actinopterygians and stem-osteichthyans[8,11]. Accordingly, the ventral expansion of the brain[27] and the higher brain-to-body mass ratio in extant lungfishes[28] and tetrapods[19] (Fig. 4) might have been permitted by the progressive reduction and displacement of the notochord posterior to the otic capsule during the evolution of each of these lineages[22,29]. However, we hypothesize that the displacement of the entire brain into the otoccipital portion, which occurs relatively late during the development of *Latimeria*, might result from biomechanical constraints linked to the intracranial joint[30].

Online content

Any methods, additional references, Nature Research reporting summaries, source data, statements of data availability and associated accession codes are available at https://doi.org/10.1038/s41586-019-1117-3.

Received: 15 October 2018; Accepted: 20 March 2019;
Published online: 17 April 2019

1. Ahlberg, P. E., Clack, J. A. & Luksevics, E. Rapid braincase evolution between *Panderichthys* and the earliest tetrapods. *Nature* **381**, 61–64 (1996).
2. Anthony, J. & Robineau, D. Sur quelques caractères juvéniles de *Latimeria chalumnae* Smith (Pisces, Crossopterygii Coelacanthidae). *C. R. Acad. Sci. Ser. D* **283**, 1739–1742 (1976).
3. Millot, J. & Anthony, J. *Anatomie de Latimeria chalumnae. II. Système Nerveux et Organes des Sens* (Centre National de la Recherche Scientifique, Paris, 1965).
4. Smith, J. L. B. A living fish of the Mesozoic type. *Nature* **143**, 455–456 (1939).
5. Kuratani, S. Development of the chondrocranium of the loggerhead turtle, *Caretta caretta*. *Zool. Sci.* **16**, 803–818 (1999).
6. de Beer, G. R. *The Development Of The Vertebrate Skull* (Univ. Chicago Press, Chicago, 1938).
7. Goodrich, E. S. *Studies on the Structure and Development of Vertebrates* Vol. 1 (Macmillan, London, 1930).
8. Clement, A. M. et al. Neurocranial anatomy of an enigmatic Early Devonian fish sheds light on early osteichthyan evolution. *eLife* **7**, e34349 (2018).
9. Janvier, P. *Early Vertebrates* (Clarendon, Oxford, 1996).
10. Lu, J. et al. The earliest known stem-tetrapod from the Lower Devonian of China. *Nat. Commun.* **3**, 1160 (2012).
11. Giles, S. & Friedman, M. Virtual reconstruction of endocast anatomy in early ray-finned fishes (Osteichthyes, Actinopterygii). *J. Paleontol.* **88**, 636–651 (2014).
12. Lu, J. et al. A Devonian predatory fish provides insights into the early evolution of modern sarcopterygians. *Sci. Adv.* **2**, e1600154 (2016).
13. Yu, X. A new porolepiform-like fish, *Psarolepis romeri*, gen. et sp. nov. (Sarcopterygii, Osteichthyes) from the Lower Devonian of Yunnan, China. *J. Vertebr. Paleontol.* **18**, 261–274 (1998).
14. Andrews, S. M., Long, J. A., Ahlberg, P. E., Barwick, R. E. & Campbell, K. The structure of the sarcopterygian *Onychodus jandemarrai* n. sp. from Gogo, Western Australia: with a functional interpretation of the skeleton. *Trans. R. Soc. Edinb. Earth Sci.* **96**, 197–307 (2006).
15. Kuratani, S., Adachi, N., Wada, N., Oisi, Y. & Sugahara, F. Developmental and evolutionary significance of the mandibular arch and prechordal/premandibular cranium in vertebrates: revising the heterotopy scenario of gnathostome jaw evolution. *J. Anat.* **222**, 41–55 (2013).
16. Kuratani, S. The neural crest and origin of the neurocranium in vertebrates. *Genesis* **56**, e23213 (2018).
17. Clack, J. A. in *Major Events in Early Vertebrate Evolution (Systematics Association Special Volume Series 61)* (ed. Ahlberg, P. E.) 392–505 (Taylor and Francis, London, 2001).
18. Kemp, A. Ontogeny of the skull of the Australian lungfish *Neoceratodus forsteri* (Osteichthyes: Dipnoi). *J. Zool. (Lond.)* **248**, 97–137 (1999).
19. Nieuwenhuys, R. et al. (eds) *The Central Nervous System of Vertebrates* Vols 1–3 (Springer, Berlin, Germany, 1998).
20. Maisey, J. G. in *Major Events in Early Vertebrate Evolution (Systematics Association Special Volume Series 61)* (ed. Ahlberg, P. E.) 263–288 (Taylor and Francis, London, 2001).
21. Kemp, A. Early development of neural tissues and mesenchyme in the Australian lungfish *Neoceratodus forsteri* (Osteichthyes: Dipnoi). *J. Zool. (Lond.)* **250**, 347–372 (2000).
22. Ahlberg, P. E., Clack, J. A., Lukševičs, E., Blom, H. & Zupiņs, I. *Ventastega curonica* and the origin of tetrapod morphology. *Nature* **453**, 1199–1204 (2008).
23. Mee-Mann, C. *The Braincase of* Youngolepis, *a Lower Devonian Crossopterygian from Yunnan, South-Western China*. PhD thesis, Univ. Stockholm and Swedish Museum of Natural History (1982).
24. Pradel, A. et al. Skull and brain of a 300-million-year-old chimaeroid fish revealed by synchrotron holotomography. *Proc. Natl Acad. Sci. USA* **106**, 5224–5228 (2009).
25. Kruska, D. C. T. The brain of the basking shark (*Cetorhinus maximus*). *Brain Behav. Evol.* **32**, 353–363 (1988).
26. Dupret, V., Sanchez, S., Goujet, D., Tafforeau, P. & Ahlberg, P. E. A primitive placoderm sheds light on the origin of the jawed vertebrate face. *Nature* **507**, 500–503 (2014).
27. Clement, A. M., Nysjö, J., Strand, R. & Ahlberg, P. E. Brain–endocast relationship in the Australian lungfish, *Neoceratodus forsteri*, elucidated from tomographic data (Sarcopterygii: Dipnoi). *PLoS ONE* **10**, e0141277 (2015).
28. Northcutt, R. G., Neary, T. J. & Senn, D. G. Observations on the brain of the coelacanth *Latimeria chalumnae*: external anatomy and quantitative analysis. *J. Morphol.* **155**, 181–192 (1978).
29. Clement, A. M. & Ahlberg, P. E. The first virtual cranial endocast of a lungfish (Sarcopterygii: Dipnoi). *PLoS ONE* **9**, e113898 (2014).
30. Dutel, H., Herbin, M., Clément, G. & Herrel, A. Bite force in the extant coelacanth *Latimeria*: the role of the intracranial joint and the basicranial muscle. *Curr. Biol.* **25**, 1228–1233 (2015).

Acknowledgements We thank R. Bills and A. Paterson (South African Institute for Aquatic Biodiversity (SAIAB)) for the loan of the fetus; and D. Neumann (Zoologische Staatssammlung München (ZSM)) for the loan of P2; M. Garcia Sanz for micro-computed tomography scanning of the adult specimen at 'AST-RX, plate-forme d'accès scientifique à la tomographie à rayons X' in the 'UMS 2700 Outils et Méthodes de Systématique intégrative CNRS-MNHN'; the European Synchrotron Radiation Facility (ESRF) for granting beam time to H.D. on ID19 for performing the PPC-SRμCT acquisitions (Proposal EC-1023); C. Bens and A. Verguin of the Collections de Pièces anatomiques en Fluides at the Muséum National d'Histoire Naturelle (MNHN) for their help; and É. Heude (MNHN) and P. Gueriau (University of Lausanne) for their comments and input on an earlier version of the draft. This work was supported by a grant from Agence Nationale de la Recherche under the LabEx ANR-10-LABX-0003-BCDiv, in the program 'Investissements d'avenir' n\u0001 ANR-11-IDEX-0004-02. H.D. was supported by a BBSRC grant (BB/M008525/1).

Reviewer information *Nature* thanks Per Ahlberg and Matt Friedman for their contribution to the peer review of this work.

Author contributions H.D., G.C., M.H., A.H. and P.J. designed the research. H.D. and P.T. made the PPC-SRμCT acquisitions. H.D., G.C. and M.H. made the conventional microtomographical acquisitions with the assistance of local staff. M.D.S. made the magnetic resonance imaging acquisitions. H.D. segmented the scans and made the three-dimensional rendering of all of the developmental stages, with the assistance of M.G. J.A.L. provided fossil material for comparative study and provided input for the discussion. M.J.F. and A.H. provided input for the results and discussion. H.D. wrote the manuscript, and made the figures and scientific illustrations. All other authors provided critical comments and were involved in the writing of the manuscript. All authors accepted the final version of the manuscript.

Competing interests The authors declare no competing interests.

Additional information
Extended data is available for this paper at https://doi.org/10.1038/s41586-019-1117-3.
Supplementary information is available for this paper at https://doi.org/10.1038/s41586-019-1117-3.
Reprints and permissions information is available at http://www.nature.com/reprints.
Correspondence and requests for materials should be addressed to H.D.
Publisher's note: Springer Nature remains neutral with regard to jurisdictional claims in published maps and institutional affiliations.

METHODS

Material. All of the specimens were obtained from public natural history collections, and no specimens were collected in the field for this project. No statistical methods were used to predetermine the sample size, which was determined according to the availability of the specimens in the natural history collections. The experiments were not randomized, and the investigators were not blinded to allocation during experiments and outcome assessment. For each specimen, we provide the collection number given by the institution in which the specimens are housed, as well as the Coelacanth Conservation Council (CCC) number. Further details on the specimens used in this study can be found in the updated inventory of all known specimens of *Latimeria* spp.[31], using the CCC number. Because no staging table of *Latimeria* development is available, the developmental stages are ordered relative to their size. The earliest developmental stage of *L. chalumnae* known so far is a 5-cm-long fetus (SAIAB 76199) (Fig. 1a). The specimen is preserved in a solution of ethanol (70%), and is housed in the collection of the SAIAB. The specimen was found in the oviduct of a large female registered as CCC 202[31], which was caught on 12 January 2005 in Kange reef, Tanzania[32]. The female was carrying 36 fetuses, but all of the rest of the fetuses appear to have been lost. The specimen was loaned to the MNHN for imaging under CITES permit 125502. P1 (MNHN C26.5 (CCC 29.5)) (Fig. 1a) is a 30.5-cm long individual with a yolk sac, preserved in formalin (7%) and housed in the Collections de Pièces anatomiques en Fluides at the MNHN. The specimen weighs 0.530 g and was found in the oviduct of a female caught on 8 January 1962, offshore of Anjouan, Comoro Islands[31]. The specimen was estimated to be 12 months old on the basis of observations of the growth lines on the surface of the scales[33]. P2 (ZSM 28409 (CCC 162.21)) (Fig. 1a) is older than P1 as the yolk sac is resorbed; the specimen is housed at the ZSM. This specimen measures 35.6 cm in length and weighs 417 g. The specimen was found in the oviduct of a female (CCC 162) caught on 11 August 1991, offshore of Quelimane, Mozambique[31]. The specimen was fixed in formalin, and preserved in this fixative until 2010 before being transferred to a solution of ethanol (75%). When transferred from formalin to ethanol, the specimen passed through a 20%, 40% and 60% ethanol solution before being put in 75% ethanol. The juvenile (MNHN C79 (CCC 94)) (Fig. 1a) is a female that measures 42 cm and weighs 800 g. The specimen is preserved in formalin (6 to 7%) and housed in the Collections de Pièces anatomiques en Fluides at the MNHN. The specimen was caught on 18 August 1974, near Iconi, Comoro Islands[2,31]. The specimen was estimated to be six months postpartum[33]. The adult specimen, housed in the Collections de Pièces anatomiques en Fluides at the MNHN, is preserved in formalin (8%). The specimen is a male (MNHN C24 (CCC 27)) (Fig. 1a) that measures 132 cm and weighs 38 kg. This specimen was caught on 4 August 1961, offshore of Grande Comoro, Comoro Islands[31].

Tomography. The fetus, P1 and P2 were imaged using long-distance PPC-SRμCT on the beam line ID19 at the ESRF. Details of the protocol followed for the PPC-SRμCT acquisitions are provided in Extended Data Table 2. The adult specimen (MNHN C24 (CCC 27)) was scanned using a micro-computed tomography scanner (Phoenix v|tome|x 240 L, General Electric) at the ASTR-X facility of the MNHN, following a previously published protocol[34,35]. Two magnetic resonance imaging (MRI) acquisitions were performed on the brain and the whole head of the juvenile (MNHN C79 (CCC 94)) at the Institut du Cerveau et de la Moelle Épinière. The MRI of the juvenile brain (MNHN C79 (CCC 94)) was performed at 11.7 T with a Bruker Biospec System (Bruker) running Paravision 6.0.1. A 72-mm birdcage resonator was used for emission (Bruker) and a 4-channel phased-array coil was used for signal reception (Bruker). The specimen was placed in a vial containing distilled water. The vial was stuck to the reception coil. Images were then acquired with a three-dimensional flash sequence with an isotropic resolution of 40 μm. Parameters were: field of view = 3.84 cm × 1.28 cm × 1.28 cm; matrix size = 960 × 320 × 320; repetition time/echo time (TR/TE) (in ms) = 40/6.4; flip angle = 15°; spectral width = 100 kHz; number of averages = 74; and total acquisition time 84 h and 11 min. MRI of the head of the juvenile (MNHN C79 (CCC 94)) was performed at 11.7 T with a Bruker Biospec System (Bruker) running Paravision 6.0.1. A 72-mm birdcage resonator was used for both emission and reception (Bruker). The specimen was directly positioned inside the resonator without any vial or liquid. Images were then acquired with a three-dimensional flash sequence with an isotropic resolution of 130 μm. Parameters were: field of view = 10.4 cm × 83.2 cm × 6.66 cm; matrix size = 800 × 640 × 512; TR/TE (in ms) = 12/5.13; flip angle = 10°; spectral width = 100 kHz; number of averages = 24; and total acquisition time 26 h and 13 min. The portions of the skull roof that were removed during the dissection (Extended Data Fig. 5) and are still preserved in the collections of the MNHN were replaced onto the skull before the MRI.

Segmentation and three-dimensional rendering. The segmentation of all of the specimens was performed in Mimic 15 and 17 (Materialise). After segmentation, STL files were imported in Cinema 4D Studio 15 (Maxon Computer) for rendering. The juvenile was dissected in 1974, and the brain was extracted from the endocranial cavity[2]. Once segmented, the brain of the juvenile was virtually replaced in its endocranial cavity, based on anatomical references obtained from the photographs taken during the dissection of the specimen in 1974, and showing the position of the brain in situ within the endocranial cavity (Extended Data Fig. 5). The skull roof, the cavity for the rostral organ and the portion of the endocranial cavity posterior to the rostral organ were destroyed during the dissection. To estimate the endocranial volume in the juvenile, these portions have been virtually restored in Meshmixer (Autodesk) based on P2. The right nasal capsule was mirrored to reconstruct its left counterpart, because the low contrast in this region did not allow for the segmentation of this structure. In all of the virtual reconstructions, we choose to display the cranial nerves on the right-hand side of the brain. When some nerves were not observable on this side of the skull, nerves located on the left-hand side of the brain were segmented and mirrored relative to the sagittal plane.

Reporting summary. Further information on research design is available in the Nature Research Reporting Summary linked to this paper.

Data availability

The PPC-SRμCT acquisitions are available online at http://paleo.esrf.eu. All surface files are deposited online at http://phenome10k.org. Any other relevant data are available from the corresponding author upon reasonable request.

31. Nulens, R., Scott, L. & Herbin, M. *An Updated Inventory of All Known Specimens of the Coelacanth* Latimeria *spp.* Smithiana Special Publication 3 (South African Institute for Aquatic Biodiversity, Grahamstown, 2011).
32. Benno, B. et al. Coelacanth (*Latimeria chalumnae* Smith, 1939) discoveries and conservation in Tanzania. *S. Afr. J. Sci.* **102**, 486–490 (2006).
33. Hureau, J.-C. & Ozouf, C. Détermination de l'âge et croissance du coelacanthe *Latimeria chalumnae* Smith, 1939 (Poisson. Crossopterygien, Coelacanthidé). *Cybium* **2**, 129–137 (1977).
34. Dutel, H., Herrel, A., Clément, G. & Herbin, M. A reevaluation of the anatomy of the jaw-closing system in the extant coelacanth *Latimeria chalumnae*. *Naturwissenschaften* **100**, 1007–1022 (2013).
35. Dutel, H., Herrel, A., Clément, G. & Herbin, M. Redescription of the hyoid apparatus and associated musculature in the extant coelacanth *Latimeria chalumnae*: functional implications for feeding. *Anat. Rec.* **298**, 579–601 (2015).

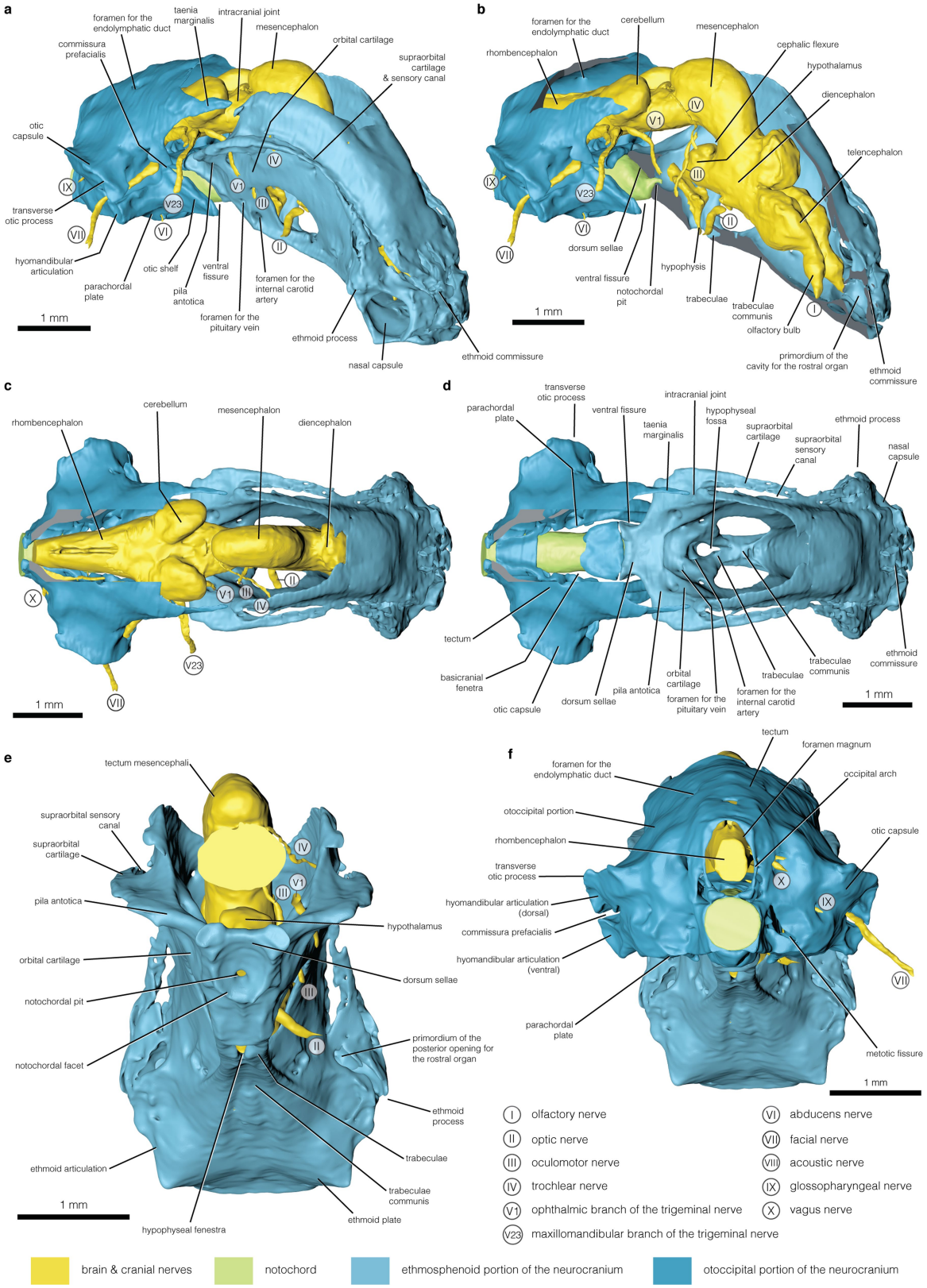

Extended Data Fig. 1 | The neurocranium of the fetus of *L. chalumnae*. **a**, **b**, The neurocranium in right anterolateral view, with the ethmosphenoid portion virtually cut open along the mid-sagittal plane in **b**. **c**, **d**, Dorsal view of the neurocranium with the roof of the otoccipital portion virtually cut open. The brain is shown in position in **c**, and was digitally removed in **d** to show the underlying neurocranial structures. **e**, Posterior view of the ethmosphenoid portion. **f**, Posterior view of the otoccipital portion.

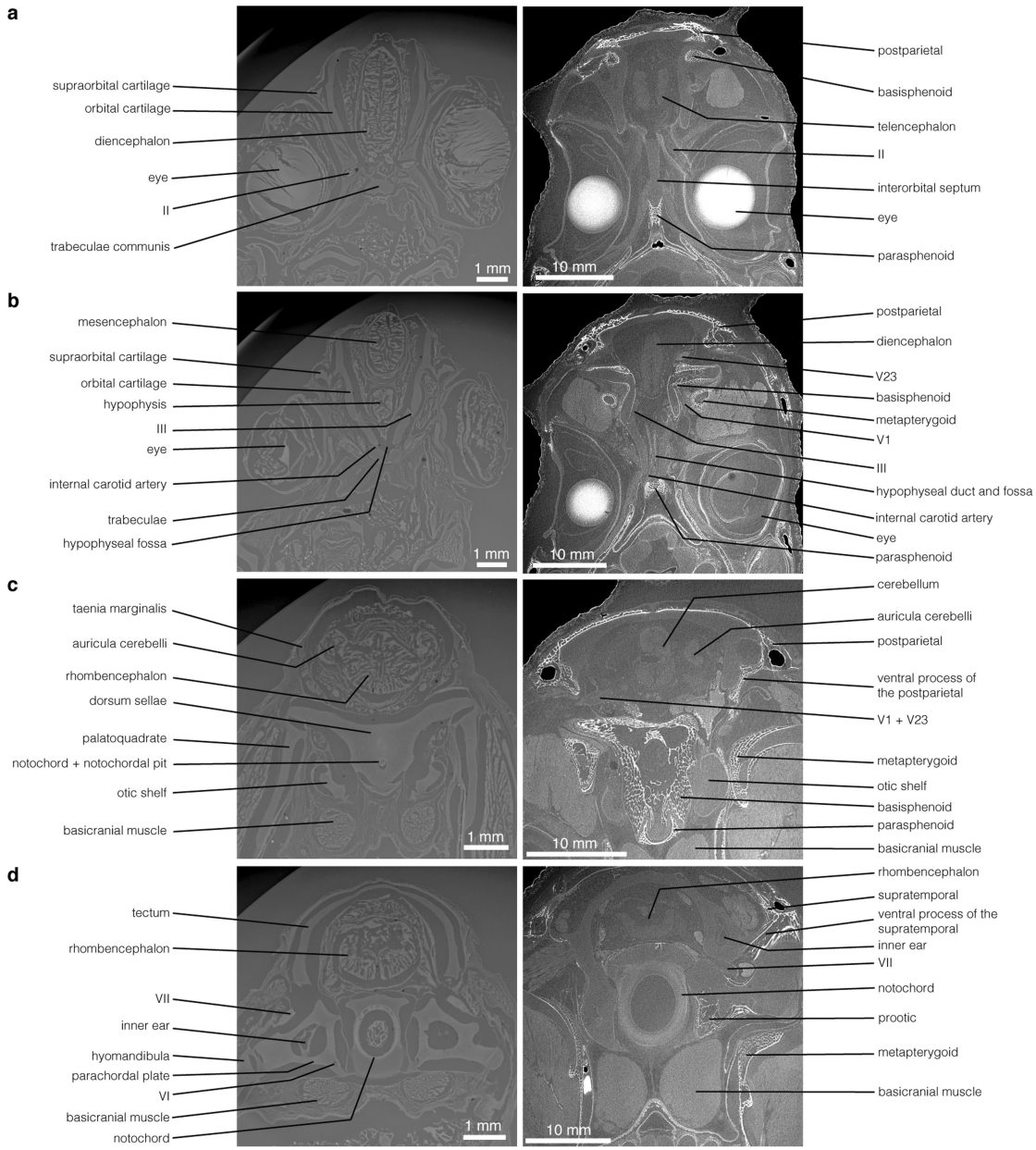

Extended Data Fig. 2 | Comparison of the neurocranium between the fetus and P1 of *L. chalumnae*. Coronal sections obtained from PPC-SRμCT acquisition along the head of the fetus (left column) and P1 (right column) of *L. chalumnae*. **a**, Section at the level of the orbital foramen. **b**, Section at the level of the hypophyseal fossa. **c**, Section at the level of the basisphenoid–palatoquadrate joint. **d**, Section at the level of the inner ear. Sample size for each stage, $n = 1$.

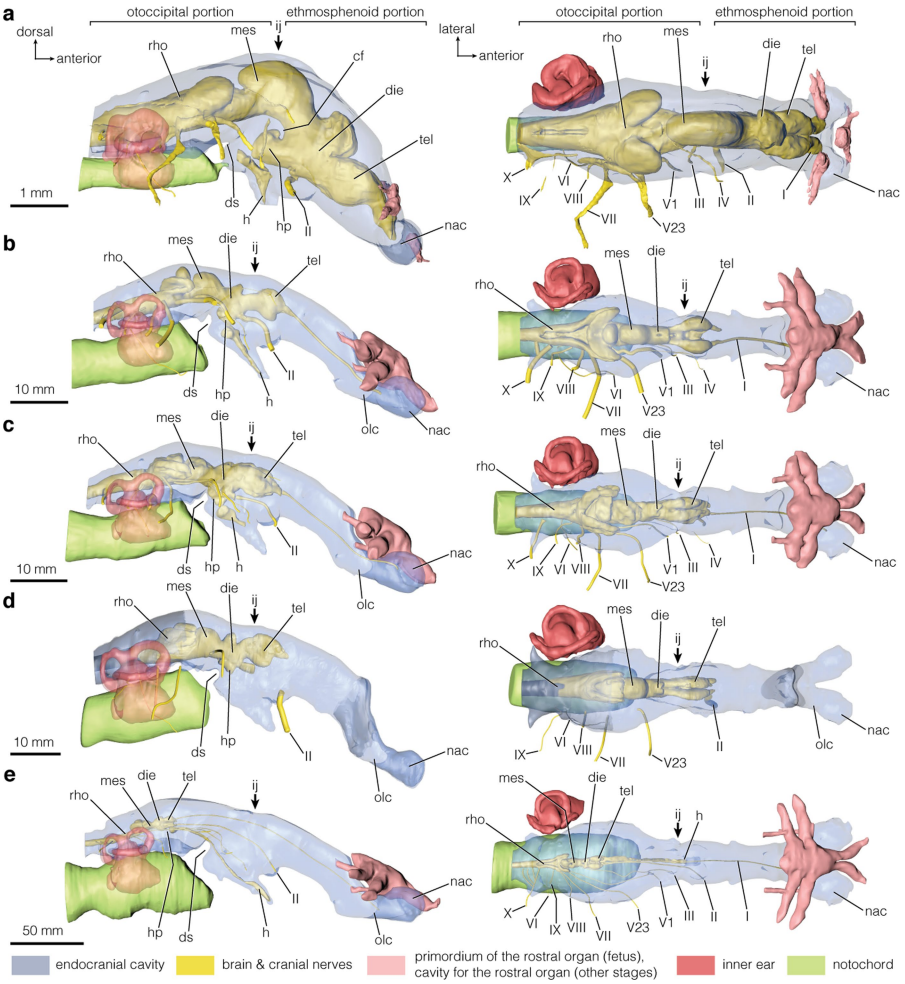

Extended Data Fig. 3 | Endocranium and brain morphology in *L. chalumnae* growth series. a–e, The fetus (**a**), P1 (**b**), P2 (**c**), juvenile (**d**) and adult (**e**) in right lateral (left) and dorsal (right) views. Grey portions in the juvenile (**d**) were reconstructed based on P2 (**c**). The rostral organ was not reconstructed in **d**, because it had been destroyed in the dissection of this specimen. IX, glossopharyngeal nerve. Sample size for each stage, $n = 1$.

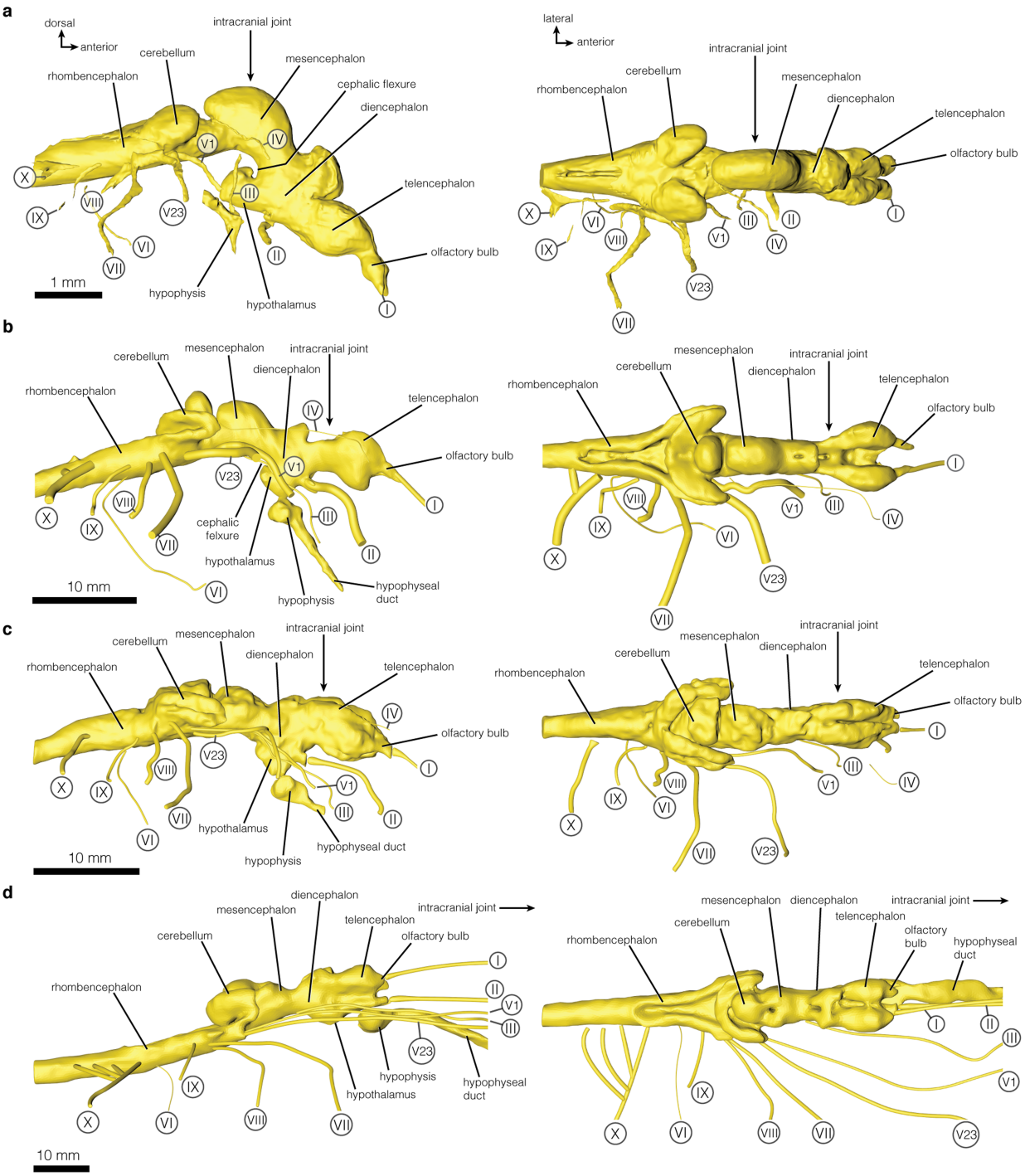

Extended Data Fig. 4 | The brain of *L. chalumnae* at different stages of development. a–d, The brains of the fetus (**a**), P1 (**b**), P2 (**c**) and adult (**d**) are shown in right lateral view (left) and dorsal (right) views. The brain of the juvenile is not displayed, because it was extracted from the endocranium and was not imaged in situ. Sample size for each stage, $n = 1$.

Extended Data Fig. 5 | The brain of the juvenile in situ. Photograph taken during the dissection of the juvenile (MNHN C79 (CCC 94)) in 1974 at the MNHN. As in earlier developmental stages, the brain spans the intracranial joint (indicated by the needle) in the juvenile. Scale in centimetres.

Extended Data Table 1 | Morphometric measurements of the notochord, brain and endocranial cavity

	Brain			Notochord		Endocranial cavity	
Stage	Volume	% adult size	% endocranial volume	Volume	% adult size	Volume	% adult size
A	1972.58	100.00	0.98	105832.33	100.00	201276.44	100.00
J	736.68*	37.34	11.21	2173.31	2.05	6566.49*	3.26
P2	475.42	24.10	12.24	1124.91	1.06	3883.14	1.93
P1	435.07	22.06	11.53	999.91	0.94	3774.35	1.83
F	2.76	0.13	28.43	0.56	< 0.10	9.707	< 0.10

All volumes are in mm^3. Asterisks indicate structures for which the missing portions have been digitally restored in the juvenile before making the measurements. A, adult; F, fetus; J, juvenile.

Extended Data Table 2 | Protocols of the PPC-SRμCT acquisitions

	Foetus	P1 & P2
Collection number	SAIAB76199	MNHN C26.5 & ZSM 28409
Voxel size (µm)	6.5	30.45
Optics	Hasselblad 100mm / 210mm	Hasselblad cinema optic
Average energy (keV)	35	63.2
Filters (mm)	Al 2 Cu 0.1	Al 2 Cu 0.25 W 0.25
Propagation distance (mm)	3000	2800
Sensor	FReLoN 2K14	FReLoN 2K14
Scintillator	LuAG:Ce 200um	LuAG:Ce 750um
Insertion device	U17.6	W150
ID Gap (mm)	14	70
Projection number	3000	4998
Scan geometry	360°, half-acquisition, vertical series 5mm	360°, half-acquisition, vertical series 7 mm
Exposure time (s)	0.2	0.1
Time per scan (min)	11.3	9.8
Reconstruction	phase retrieval	phase retrieval

Scans were performed on beam line ID19 at the ESRF.

nature research

Corresponding author(s): Hugo Dutel

Last updated by author(s): 11/02/2019

Reporting Summary

Nature Research wishes to improve the reproducibility of the work that we publish. This form provides structure for consistency and transparency in reporting. For further information on Nature Research policies, see Authors & Referees and the Editorial Policy Checklist.

Statistics

For all statistical analyses, confirm that the following items are present in the figure legend, table legend, main text, or Methods section.

n/a	Confirmed
☐	☒ The exact sample size (*n*) for each experimental group/condition, given as a discrete number and unit of measurement
☒	☐ A statement on whether measurements were taken from distinct samples or whether the same sample was measured repeatedly
☒	☐ The statistical test(s) used AND whether they are one- or two-sided *Only common tests should be described solely by name; describe more complex techniques in the Methods section.*
☒	☐ A description of all covariates tested
☒	☐ A description of any assumptions or corrections, such as tests of normality and adjustment for multiple comparisons
☒	☐ A full description of the statistical parameters including central tendency (e.g. means) or other basic estimates (e.g. regression coefficient) AND variation (e.g. standard deviation) or associated estimates of uncertainty (e.g. confidence intervals)
☒	☐ For null hypothesis testing, the test statistic (e.g. *F*, *t*, *r*) with confidence intervals, effect sizes, degrees of freedom and *P* value noted *Give P values as exact values whenever suitable.*
☒	☐ For Bayesian analysis, information on the choice of priors and Markov chain Monte Carlo settings
☒	☐ For hierarchical and complex designs, identification of the appropriate level for tests and full reporting of outcomes
☒	☐ Estimates of effect sizes (e.g. Cohen's *d*, Pearson's *r*), indicating how they were calculated

Our web collection on statistics for biologists contains articles on many of the points above.

Software and code

Policy information about availability of computer code

Data collection	For synchrotron tomographic data reconstruction, we used the ESRF software PyHST2. Data concatenation and formatting was performed with dedicated codes in Matlab 7 (available at the ESRF). The software MIMICS was used to segment the data. Rendering of the models was made in Cinema 4D 15.
Data analysis	ESRF software PyHST2, Matlab 7, MIMICS 15 & 17, Cinema 4D 15.

For manuscripts utilizing custom algorithms or software that are central to the research but not yet described in published literature, software must be made available to editors/reviewers. We strongly encourage code deposition in a community repository (e.g. GitHub). See the Nature Research guidelines for submitting code & software for further information.

Data

Policy information about availability of data

All manuscripts must include a data availability statement. This statement should provide the following information, where applicable:

- Accession codes, unique identifiers, or web links for publicly available datasets
- A list of figures that have associated raw data
- A description of any restrictions on data availability

Tomographic data from the ESRF will be publicly accessible on the open access ESRF database (http://paleo.esrf.eu). Surface files (PLYs) will be publicly accessible on http://phenome10k.org.
Restriction on data availability: Please cite the original articles linked to the data you are using, as well as the repository institutions and the public databases. Non-commercial use only, no distribution to third-party.

Field-specific reporting

Please select the one below that is the best fit for your research. If you are not sure, read the appropriate sections before making your selection.

☐ Life sciences ☐ Behavioural & social sciences ☒ Ecological, evolutionary & environmental sciences

For a reference copy of the document with all sections, see nature.com/documents/nr-reporting-summary-flat.pdf

Ecological, evolutionary & environmental sciences study design

All studies must disclose on these points even when the disclosure is negative.

Study description	We describe the neurocranial structures in different developmental stages of the coelacanth Latimeria chalumnae.
Research sample	5 specimens (= 5 developmental stages) of the coelacanth Latimeria chalumnae. Sample size was determined based on the specimens available in natural history collections. The specimens are all housed in the natural history collections of public institutions, and all have a collection number. Details on the specimens are provided below and in supplementary information. No new specimens were collected on the field for the present study.
Sampling strategy	Sample size was determined based on the specimens available in natural history collections, and their preservation. 5 specimens representing 5 different developmental stages of L. chalumnae were sampled. To our knowledge, this is to date the most extensive growth series gathered for L. chalumnae. Information on the specimens are provided below in Animals and other organisms Section, as well as in Supplementary information. No statistical methods were used in the present study and no sample-size calculation was performed.
Data collection	Tomography using conventional (by technical staff at the MNHN) and synchrotron (by PT and HD) sources, as well as MRI (by MS). HD segmented all the scans, and produced the 3D reconstructions.
Timing and spatial scale	Timing and spatial scale were not relevant and applicable to the analyses.
Data exclusions	No data were excluded from the analyses.
Reproducibility	Digital reconstructions of the specimens were obtained from tomographical data. We did not repeated the tomographical acquisitions because of: the length of the tomographical acquisitions, the fragility of the material studied, and/or the necessity to keep the X-ray dose as low as possible. Raw tomographical slices will be available on public depositories, allowing our peers to make direct observations and to segment the image stacks.
Randomization	Due to sample size, randomization was not relevant to the study. No statistical analyses were performed.
Blinding	Due to sample size, blinding was not relevant to the study. No statistical analyses were performed.

Did the study involve field work? ☐ Yes ☒ No

Reporting for specific materials, systems and methods

We require information from authors about some types of materials, experimental systems and methods used in many studies. Here, indicate whether each material, system or method listed is relevant to your study. If you are not sure if a list item applies to your research, read the appropriate section before selecting a response.

Materials & experimental systems

n/a	Involved in the study
☒	☐ Antibodies
☒	☐ Eukaryotic cell lines
☒	☐ Palaeontology
☐	☒ Animals and other organisms
☒	☐ Human research participants
☒	☐ Clinical data

Methods

n/a	Involved in the study
☒	☐ ChIP-seq
☒	☐ Flow cytometry
☐	☒ MRI-based neuroimaging

Animals and other organisms

Policy information about studies involving animals; ARRIVE guidelines recommended for reporting animal research

Laboratory animals	No laboratory animals were used in this study.
Wild animals	The specimens are all housed in the natural history collections of public institutions. For each specimen, we provide the

Wild animals	specimen collection number given by the host institution, as well as the Coelacanth Conservation Council (CCC) number. Further details on the specimens used in this study can be found in the updated inventory of all known specimens of Latimeria spp. (Nulens et al 2011 - Smithinia Special Publication 3, 12 September 2011), using the CCC number. The earliest developmental stage of L. chalumnae known so far is a 5 cm long fetus (SAIAB 76199). The specimen is preserved in a solution of ethanol (70%), and housed in the collection of the SAIAB, Grahamstown, South Africa. The specimen was found in the oviduct of a large female registered as CCC 202 (Nulens et al 2011), caught on January 12, 2005 in Kange reef, Muheza District, Tanzania (Benno et al 2006). The female was carrying 36 fetuses but all the rest of the fetuses appear to have been lost. The specimen was loaned to the MNHN, France for imaging under the CITES permit 125502. The first pup P1 (MNHN C26.5, CCC 29.5) is a 30.5 cm long individual with a yolk sac, preserved in formalin (7 %) and housed in the Collections de Pièces anatomiques en Fluides at the MNHN, Paris. The specimen weighs 0.530 g and was found in the oviduct of a female caught on January 8, 1962, offshore Anjouan, Comoro Islands. The specimen was estimated to be 12 months old based on the observation of the growth lines on the surface of the scales (Hureau & Ozouf 1977). The second pup P2 (ZSM 28409, CCC 162.21) is older than P1 as the yolk sac is resorbed, and housed at the Zoologische Staatssammlung München, Germany. This specimen measures 35.6 cm in length and weighs 417 g. The specimen was found in the oviduct of a female (CCC 162) caught on August 11, 1991, offshore Quelimane, province of Zambezia, Mozambique. The specimen was fixed in formalin, and preserved in this fixative until 2010 before being transferred to a solution of ethanol (75 %). When transferred from formalin to ethanol, the specimen passed through a 20 %, 40 %, and 60 % ethanol solution before being put in 75 % ethanol. The juvenile (MNHN C79, CCC 94) is a female that measures 42 cm and weighs 800 g. The specimen is preserved in formalin (6 to 7 %) and housed in the Collections de Pièces anatomiques en Fluides at the MNHN, Paris. The specimen was caught on August 18, 1974, near Iconi, Comoro Islands. The specimen was estimated to be 6-months postpartum (Hureau & Ozouf 1977). The adult specimen (A1), housed in the Collections de Pièces anatomiques en Fluides at the MNHN, Paris, is preserved in formalin (8 %). The specimen is a male (MNHN C24, CCC 27) that measures 132 cm and weighs 38 kg. This specimen was caught on August 4, 1961 offshore Grande Comoro, Comoro Islands.
Field-collected samples	No specimens were collected on the field for this study. Digital reconstructions are only based on specimens housed in museum collections. Provenance and deposition of specimens is provided above and in the supplementary information.
Ethics oversight	No ethic guidance was necessary for this study. The fetus of L. chalumnae (5 cm stage) was sent from South Africa to France for PPC-SRμCT under the CITES permit 125502 provided by SAIAB. The specimen has been returned to its institution after the experiment.

Note that full information on the approval of the study protocol must also be provided in the manuscript.

Magnetic resonance imaging

Experimental design

Design type	MRI of formalin fixed brain and whole head of a juvenile specimen of L. chalumnae.
Design specifications	NA
Behavioral performance measures	NA

Acquisition

Imaging type(s)	Structural
Field strength	11.7 T
Sequence & imaging parameters	MRI was performed with a Bruker Biospec System (Bruker, Germany). Isolated brain: A 72-mm birdcage resonator was used for emission (Bruker, Germany) and a 4-channel phased-array coil was used for signal reception (Bruker, Germany). Images were acquired with a 3D Flash sequence with an isotropic resolution of 40 µm. Field of View = 3.84*1.28*1.28 cm3; Matrix size = 960*320*320; TR/TE (ms) = 40/6.4; Flip Angle = 15°; Spectral Width = 100 kHz; Number of averages = 74; Total acquisition time = 84 hours and 11 minutes; Whole head: A 72-mm birdcage resonator was used for both emission and reception (Bruker, Germany). Images acquired with a 3D Flash sequence with an isotropic resolution of 130 µm. Field of View = 10.4*83.2*6.66 cm3; Matrix size = 800*640*512; TR/TE (ms) = 12/5.13; Flip Angle = 10°; Spectral Width = 100 kHz; Number of averages = 24; Total acquisition time = 26 hours and 13 minutes.
Area of acquisition	Isolated brain of a juvenile L. chalumnae and whole head of a juvenile of L. chalumnae.

Diffusion MRI ☐ Used ☒ Not used

Preprocessing

Preprocessing software	Bruker Biospec System (Bruker, Germany) running Paravision 6.0.1.
Normalization	NA
Normalization template	NA

Noise and artifact removal: NA

Volume censoring: NA

Statistical modeling & inference

Model type and settings: NA

Effect(s) tested: NA

Specify type of analysis: ☐ Whole brain ☒ ROI-based ☐ Both

Anatomical location(s): Whole head and isolated brain of a juvenile coelacanth L. chalumnae.

Statistic type for inference (See Eklund et al. 2016): NA

Correction: NA

Models & analysis

n/a	Involved in the study
☒	☐ Functional and/or effective connectivity
☒	☐ Graph analysis
☒	☐ Multivariate modeling or predictive analysis